Advances in Science and Technology
ISSN: 1662-0356, Vol. 99, pp 69-74
doi:10.4028/www.scientific.net/AST.99.69
© 2017 Trans Tech Publications, Switzerland
Submitted: 2016-03-25
Accepted: 2016-06-27
Online: 2016-10-31

Potential Fluctuation in RRAM Based on Non-Stoichiometric Hafnium Sub-Oxides

Damir R. Islamov[1,2,a*] , Vladimir N. Kruchinin[1] , Vladimir Sh. Aliev[1] , Timofey V. Perevalov[1,2] , Vladimir A. Gritsenko[1,2,b] , Igor P. Prosvirin[3] , Oleg M. Orlov[4] and Albert Chin[5,c]

[1]Rzhanov Institute of Semiconductor Physics SB RAS, 13 Lavrentiev ave., 630090 Novosibirsk, Russian Federation

[2]Novosibirsk State University, 2 Pirogova str., 630090 Novosibirsk, Russian Federation

[3]Boreskov Institute of Catalysis SB RAS, 5 Lavrentiev ave., 630090, Novosibirsk, Russian Federation

[4]JSC Molecular Electronics Research Institute, 1st Zapadny proezd 12/1, 124460 Zelenograd, Russian Federation

[5]National Chiao Tung University, Hsinchu 300, Taiwan

[a]damir@isp.nsc.ru, [b]grits@isp.nsc.ru, [c]achin@faculty.nctu.edu.tw

Keywords: hafnium sub-oxides, RRAM, ReRAM, low resistance state, fluctuations.

Abstract. We study the structure of nonstoichiometric HfO_x films with variable composition using methods of XPS, spectroscopic ellipsometry, and *ab initio* calculations. According to XPS and optical absorption experiment data HfO_x consists of metal Hf and 10-15% of nonstoichiometric hafnium sub-oxide HfO_y ($y < 2$). HfO_y can be placed between HfO_2 and Hf, inside HfO_2, inside Hf. According to this model space fluctuations of chemical composition cause space fluctuations of bandgap in HfO_x. We found that transport in such electronic systems is described by percolation theory. This approach can be applied to explain LRS transport of HfO_x-based RRAM.

Introduction

In modern silicon devices SiO_2 is superseded by high-κ dielectrics, such as HfO_2, ZrO_2, Ta_2O_5 etc. Hafnia (HfO_2) permittivity depends on the modification, varies in the range of 16–40. HfO_2 is the promising material for CMOS devices, DRAM capacitors, non-volatile memory devices [1]. Of great interest is the use of nonstoichiometric hafnium sub-oxides HfO_x ($x < 2$). Variation of HfO_x chemical composition (stoichiometry) leads to changes in its electronic structure, which opens up the possibility of controlling optical and electrical (conductivity) properties. Coordination numbers of Hf and O atoms in HfO_2 are high in compare with compounds of silica SiO_x. Thus, is not clear what is the model which describes the structure of non-stoichiometric HfO_x. The goals of this contribution is to study the atomic and electronic structure of HfO_x with variable composition.

Experiment

HfO_x films were produced using Hf target ion beam sputtering deposition in oxygen atmosphere. Pure Hf target was bombarded by $Ar+$ ion beam, spattered Hf particles were mixed with oxygen beam before deposition on Si wafer. The composition (x-parameter) of deposited HfO_x was defined by partial oxygen pressure. For our experiments we grew six sets of HfO_x samples at the partial oxygen pressures of $(0.44–3.6) \times 10^{-4}$ Pa. In these conditions, we produced four sets of the samples of non-stoichiometric ($x < 2$) films and two sets of almost stoichiometric composition ($x \approx 2$). Structural analysis showed that the resulting films were amorphous.

All rights reserved. No part of contents of this paper may be reproduced or transmitted in any form or by any means without the written permission of Trans Tech Publications, www.ttp.net. (#71089402-06/11/16,11:15:02)

The core-level Hf$4f_{7/2}$-Hf$4f_{5/2}$ and valence band spectra of HfO_x films were obtained using XPS machine with monochromatic $AlK\alpha$ radiation. The dispersive refractive index and absorption coefficient of HfO_x films were determined by means of spectral ellipsometry.

Transport measurements were recorded for metal-insulator-metal (MIM) structures of Si/TaN/HfO_x/Ni. These structures were fabricated by deposition of the 8-nm-thick amorphous HfO_x on 100-nm-thick TaN films on Si wafers, using physical vapor deposition. A pure HfO_2 target was bombarded by an electron beam, and HfO_2 was deposited on the wafer. No post deposition annealing was applied to produce non-stoichiometric HfO_x films. Structural analysis showed that the resulting films were amorphous. All samples for transport measurements were equipped with round 50-nm-thick Ni gates with a radius of 70 μm.

Transport measurements were performed using a Hewlett Packard 4155B Semiconductor Parameter Analyzer and an Agilent E4980A Precision LCR Meter. All measurement equipment were protected against short circuiting with the current through the sample limitation of 1 μA.

The higher-level electronic-structure calculations were performed using the density functional theory (DFT) with the QUANTUM ESPRESSO software package [2]. We adopted B3LYP hybrid functional to reproduce the accurate band gap values. The potentials of nuclei and core electrons have been expressed via pseudopotentials retaining the norm. The Bloch functions of electrons in the crystal were represented by plane wave expansions with a cutoff energy of 55 Ry. The atomic arrangement was optimized with a force convergence threshold of 0.04 eV/E. We simulated the electronic structure of monoclinic (m-) HfO_2 as the most stable crystalline hafnia phase. The 24-atom periodic hafnia supercell with 1–3 oxygen vacancies was used to simulate non-stoichiometric HfO_x. The theoretical XPS spectra were calculated by summing up the partial density of states with the weight factors equal to the corresponding photo-ionization cross sections [3].

Results and Discussions

XPS Spectra. XPS spectra of Hf$4f_{7/2}$-Hf$4f_{5/2}$ core level in some HfO_x variable composition are shown in Fig. 1(a). For HfO_x, grown at high pressures of oxygen, a peak is observed at an energy corresponding to the stoichiometric HfO_2 (dashed lines). Decreasing the oxygen pressure during HfO_x synthesis accompanied by the appearance of XPS peaks corresponding to metal Hf (dash-dotted lines). With decreasing of oxygen pressure, the intensity of the peaks corresponding to metal hafnium increases. The decomposition of the spectra indicates that in addition to HfO_2 and Hf the films have a non-stoichiometric phase of HfO_y. Corresponding to this phase peaks are located approximately in the middle between the Hf- and HfO_2-related peaks as shown in the Fig. 1(a) by dotted lines. So, according to XPS HfO_x is a mixture of stoichiometric HfO_2, metal Hf, and non-stoichiometric phase of HfO_y.

Experimental valence band spectra of HfO_x is in good agreement with simulated spectra for monoclinic m-HfO_x as shown in Fig. 1(b). A proof of the existence of non-stoichiometric hafnia in our films can be obtained from the comparison of the experimental valence-band XPS with the corresponding one calculated from the first principles for m-HfO_2 with neutral oxygen vacancy and polyvacancy (Fig. 1(b)). The calculation satisfactorily describes the experiment, with the fact that the XPS spectra are compared for HfO_x in amorphous and monoclinic phases. The presence of the neutral oxygen vacancy in m-HfO_2 leads to the defect levels at 3.2 eV above the valence-band ceil. XPS spectra of metal Hf was measure for polished surface of Hf target.

Optical Spectra. Fig. 2(a) shows the spectra of absorption coefficient for HfO_x. Bandgap of amorphous HfO_2 is $E_g = 5.6$ eV [4]. HfO_x absorption coefficient increases monotonically with increasing of photon energy in the range of 1.1–4.5 eV. At the energies higher than 4.5 eV a sharp increase of absorption coefficient is observed. In the range of 1.1–4.5 eV absorption is non-zero due to presence of Hf metallic clusters. Absorption at photon energies of > 4.5 eV is caused by presence of non-stoichiometric HfO_y.

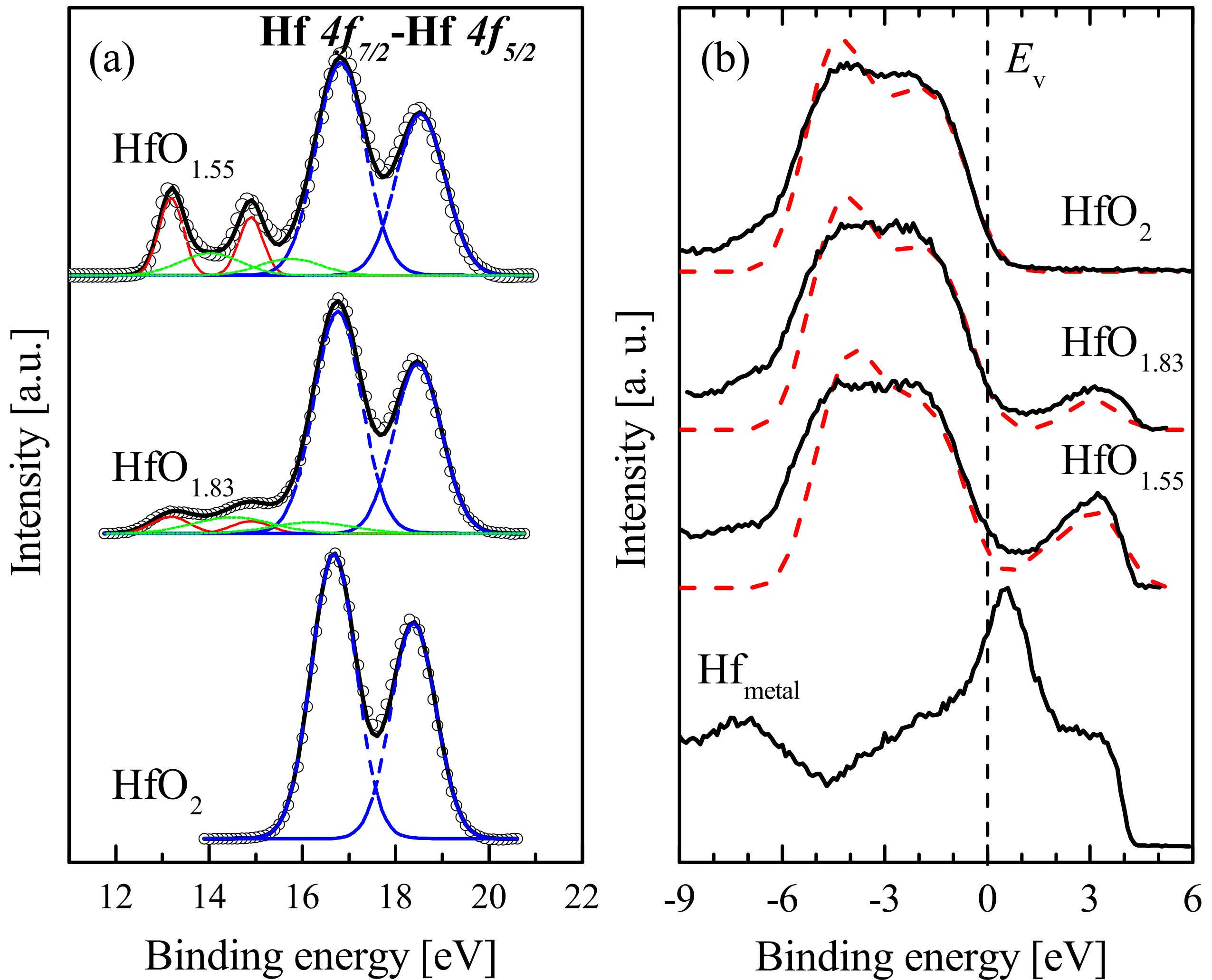

Fig. 1: (Color online) (a) Experimental (charachters) and Gauss decompositions (lines) Hf*4f* spectra of HfO_x with variable composition. Dashed lines represent Hf*4f* core levels in HfO_2, dotted — in HfO_y, dash-dotted — in Hf, solid thick lines show sums of the Gauss decompositions. (a) Experimental (solid lines) and simulated (dashed lines) valence band spectra of HfO_x with variable composition. Reference energy is the top of the valence band here.

Fig. 2(b) shows the spectra of refractive index for HfO_x. Stoichiometric HfO_2 exhibits typical for dielectrics refractive index dispersion, increasing monotonically with increasing of photon energy. Strongly non-stoichiometric $HfO_{1.55}$ has optical properties close to metal Hf (Fig. 2(a) and Fig. 2(b)). Such behavior might be caused by percolation between metal Hf and HfO_y fractions in lateral scale comparable with wave length of photons. Competition of dielectric and metal phases leads to complex non-monotonical behavior refractive index spectra of non-stoichiometric $HfO_{1.83}$.

Structure of HfO_x. According to XPS and optical absorption experiment data HfO_x consists of metal Hf and 10-15% of non-stoichiometric hafnium sub-oxide HfO_y ($y < 2$). HfO_y can be placed between HfO_2 and Hf, inside HfO_2, inside Hf. Fig. 3(a) shows planar model of HfO_x regarding the intermediate structural model [6]. According to proposed model HfO_x consists of three phases: HfO_2, HfO_y and Hf. According to this model space fluctuations of chemical composition cause spatial fluctuations of bandgap width in HfO_x. The maximal fluctuation of the energy scale is equal to the HfO_2 band gap width of $E_g = 5.6$ eV. The work function of metallic hafnium is 4.0 eV, electron affinity of HfO_2 is 2.0 eV [5]. The maximal fluctuation scale of the HfO_x conduction band is 2.0 eV, which

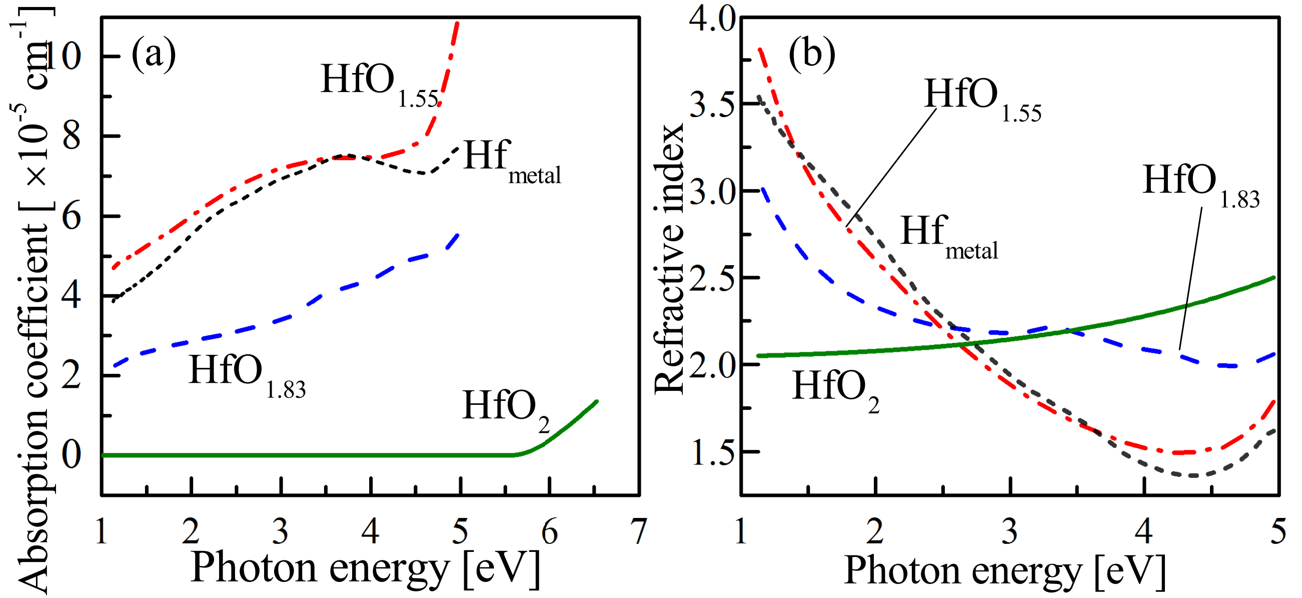

Fig. 2: (Color online) (a) Absorption coefficient and (b) befraction index spectra of HfO_x with variable composition. Solid line represents properties of HfO_2, dashed line — $HfO_1 \cdot 83$, dash-dotted line — $HfO_1 \cdot 55$, dotted line — metal Hf.

equals the electron barrier height of Hf/HfO_2 interface (Fig. 3(b)). The hole energy barrier of Hf/HfO_2 is 3.6 eV (Fig. 3(b)), which leads to the maximal fluctuation scale of the HfO_x valence band of 3.6 eV. Fig. 3(c) shows energy diagram of HfO_x. Bandgap HfO_x varies in the range of 0–5.6 eV The bottom of the conduction band Ec against the energy of an electron in a vacuum E_0 varies in the range of 2.0–4.0 eV, which leads to E_c fluctuation scope of 2.0 eV. The valence band ceiling E_v against E_0 varies in the range of 4.0–7.6 eV.

The nanoscale fluctuations at the bottom of conduction band and at the top of valence band are close to those proposed in the model developed in [8, 7], as shown in Fig. 3(d). The charge transport in such electron systems can be described according to percolation model. This model assumes that excited electrons with energy higher than the flow level E^e are delocalized, and driving round a random potential, transfer the charge. The hole conductivity is realized through the excitation of electrons with energy E^h to the Fermi level. These excitations form hole-type quasiparticles, which transfer the charge. In other words, to be involved in transport processes, electrons and holes must overcome energy thresholds ($W^{e,h}$ here, and $W^e \neq W^h$ in general). The current-voltage characteristics are exponentials [7]:

$$I(T) = I_0(T) \exp\left(\frac{(CeFaV_0^{\nu})^{\frac{1}{1+\nu}}}{kT}\right), \qquad (1)$$

where I is the current, I_0 is the preexponential factor, e is the electron charge, F is the electric field, a is the space scale of fluctuations, V_0 is the amplitude of energy fluctuation, k is the Boltzmann constant, C is a numeric constant, and ν is a critical index. The values of the constants were derived from Monte-Carlo simulations and evaluated at $C \simeq 0.25$ [7] and $\nu = 0.9$ [8]. Percolation energy threshold W can be evaluated based on the temperature dependency of the preexponential factor:

$$I_0(T) \sim \exp\left(-\frac{W}{kT}\right). \qquad (2)$$

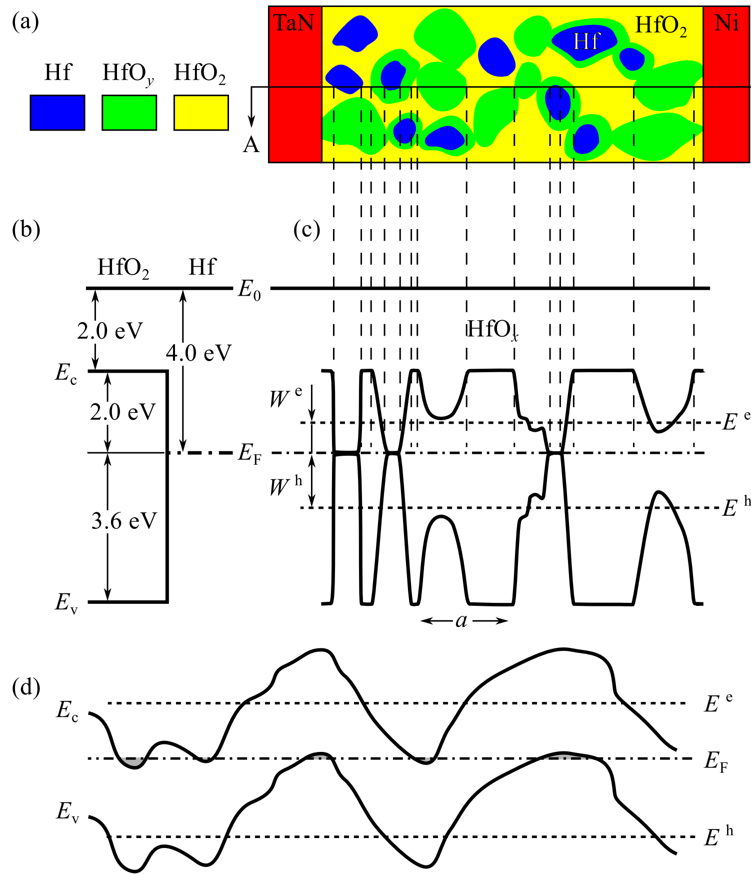

Fig. 3: (Color online) Percolation model in electron systems with the nanoscale potential fluctuations. (a) Schematic planar illustration of Hf/HfO_x ($x < 2$) space-modulated by chemical composition structure. (b) Flat band energy diagram of HfO_2/Hf structure. (c) Energy diagram of the structure with nanoscale potential fluctuations. (d) Energy diagram of large-scale potential fluctuations in a semiconductor layer [7]. $E^{e,h}$ and $W^{e,h}$ are percolation levels and percolation thresholds of the electrons and holes respectively.

Low Resistance State of HfO_x-based RRAM. As an appication of our model, we assumed that a filament in in low resistance state (LRS) of hafnia-based RRAM has the structure of non-stoichiometric HfO_x. The solid lines in Fig. 4 show the results of LRS simulations regarding the percolation model (Eq. 1). Numeric fitting returns the value of combination as $CaV_0^{0.9} = 0.45\,\mathrm{nm}\cdot\mathrm{eV}^{0.9}$, which corresponds to $V_0 = 1.9\,\mathrm{eV}$ when $a = 1\,\mathrm{nm}$ and $C = 0.25$. The slope of a fitting line in a $\ln(I_0)$-vs-T^{-1} plate according to (2) corresponds to a percolation threshold of $W \approx 1.0\,\mathrm{eV}$. Because $W \lesssim V_0 \leqslant 2.0\,\mathrm{eV}$ (for electrons), we can estimate the space size of nanoscale fluctuations as $a \approx 1$–$2\,\mathrm{nm}$.

Summary

In conclusion, we demonstrate that hafnium sub-oxides HfO_x with $x < 2$ are mixtures of stoichiometric hafnium oxides HfO_2, metal Hf, and non-stoichiometric phase of HfO_y. Decreasing stoichiometry parameter x leads to increasing absorption of photons with energies of 0–5.5 eV. The percentage of nonstoichiometric HfO_y phase weekly depends on x value. We show that charge transport in non-stoichiometric hafnium sub-oxides is described according to the percolation model in electron systems exhibiting potential nanoscale fluctuations. This approach can be applied to explain LRS conductivity in HfO_x-based RRAM structures.

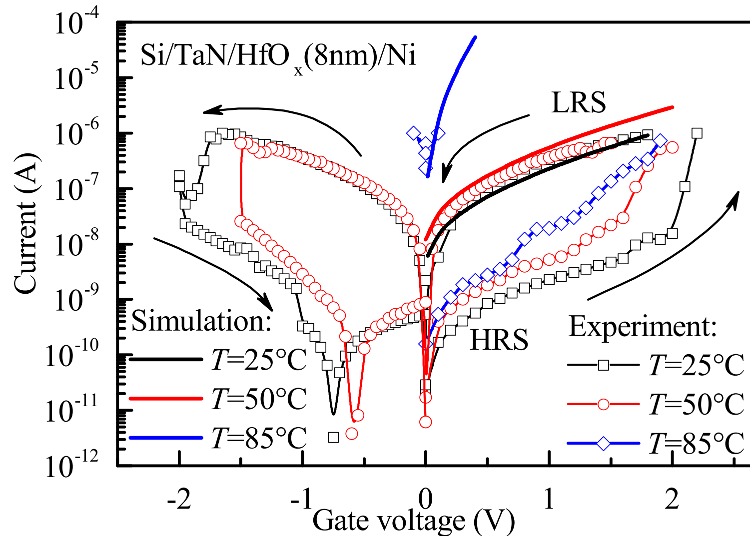

Fig. 4: (Color online) Experimental RRAM current-voltage characteristics (characters) in Si/TaN/HfO$_x$/Ni structures at different temperatures. Solid lines present LRS simulations by percolation model (Eq. 1).

Acknowledgments

This work was supported by the Russian Science Foundation (grant No. 16-19-00002), and Ministry of Science and Technology, Taiwan. The modeling was performed on a supercomputing cluster of the Institute of Semiconductor Physics, Siberian Branch of the Russian Academy of Sciences.

References

[1] S. Kar, High Permittivity Gate Dielectric Materials, Springer Series in Advanced Microelectronics 43 (2013).

[2] P. Giannozzi, S. Baroni, N. Bonini, et al., QUANTUM ESPRESSO: a modular and open-source software project for quantum simulations of materials, J. Phys. Condens. Matter 21 (2009) 395502-395520.

[3] J.J. Yeh, Atomic Calculation of Photoionization Cross-Section and Asymmetry Parameters Gordon and Breach Science Publishers, Langhorne, PE (USA), 1993.

[4] V.V. Afanas'ev, A. Stesmans, Internal photoemission at interfaces of high-κ insulators with semiconductors and metals, J. Appl. Phys. 102 (2007) 081301.

[5] W. Zheng, Kit H. Bowen Jr., Electronic Structure Differences in ZrO_2 vs HfO_2, J. Phys. Chem. A 109 (2005) 11521-11525.

[6] Y.N. Novikov, V.A. Gritsenko, Short-range order in amorphous SiO_x by x ray photoelectron spectroscopy, J. Appl. Phys. 110 (2011) 014107.

[7] B. I. Shklovskii, Percolation conductivity in strong electric fields, Sov. Phys. Semicond. 13 (1979) 53.

[8] B.I. Shklovskii, A.L. Éfros, Percolation theory and conductivity of strongly inhomogeneous media, Phys.-Usp. 18 (1975) 845-862.